Thin Solid Films 642 (2017) 151–156

Contents lists available at ScienceDirect

Thin Solid Films

journal homepage: www.elsevier.com/locate/tsf

Ultraviolet light-induced wettability control of ultrathin atomic layer deposited TiO_2 film surface

Youngmoon Jang, Byungchan Yang, Jeongwoo Shin, Jihwan An*

Department of Manufacturing Systems and Design Engineering, Seoul National University of Science and Technology, Seoul 01811, South Korea

ARTICLE INFO

Keywords:
Atomic layer deposition
Titanium dioxide
Thin films, wettability, ultraviolet surface treatment

ABSTRACT

Here, we show that the surface wettability of ultrathin (6–16 nm) TiO_2 films deposited by atomic layer deposition (ALD) can be tuned by an ultraviolet (UV) light treatment. The controllability is also shown to be largely dependent on the deposition temperature and thickness. The surface of a 16-nm-thick ALD TiO_2 film deposited at 200 °C was shown to be super-hydrophilic (water contact angle < 1°) by an UV treatment (~3 mW/cm^2) applied for only 8 min due to the photocatalytic activity of the films, while thinner films and films deposited at lower temperatures were not. Microscopic and optical characterizations prove that the difference mainly stems from the crystallinity, the bandgap energy and the defect density of the TiO_2 films.

1. Introduction

TiO_2 films are widely used in optical devices due to their high chemical stability, high transmittance, and high refractive index [1,2]. TiO_2 film is also known to have a high dielectric constant. For example, its dielectric constant can be as high as ~100 (rutile) even when it is ultra-thin (< 100 nm). TiO_2-based perovskite oxide films such as $BaTiO_3$ and $SrTiO_3$ show extremely high dielectric constants (> 100), and therefore, are thought to be attractive alternative materials for replacing SiO_2 in memory or logic devices [3–5]. More importantly, TiO_2 is being widely researched for such next-generation energy conversion devices as dye-sensitized solar cells (DSSCs) or photoelectrochemical cells due to its photocatalytic activity. For example, it is reported that the (101) plane of anatase TiO_2 is ideally suited for chemisorption with the existing sensitizers in DSSCs [6].

Photocatalytic activity at the TiO_2 surface can tune the surface property as well. When photons with energies higher than the bandgap of the material interact with the TiO_2, electron–hole pairs are generated, and the electrons and holes diffuse to the surface. Those electrons and holes near the surface may participate in the redox reaction, create radicals, and alter surface properties [7,8] by which a super-hydrophilic TiO_2 surface (water contact angle 0–1°) has been demonstrated [9]. Tuning the surface properties of TiO_2 is particularly crucial when one wants to fabricate heterostructures (e.g., nanoparticles deposited on the TiO_2 surface) for catalysts or photoelectrodes.

Among the various techniques used to fabricate TiO_2 thin films, atomic layer deposition (ALD) has been widely researched in recent years [6,10–19]. The ALD process is a kind of chemical vapor deposition process that is based on a surface-limiting chemical reaction between precursors. Compared to other thin-film deposition techniques, the ALD process offers such advantages as the ability to control the thickness of the film extremely accurately at the sub-nanometer scale, as well as the ability to deposit films or nanoparticles conformally on complex 3-dimensional surfaces. Therefore, TiO_2 films deposited by ALD can be easily applied to nanostructures with high surface areas, realizing high-performance photocatalytic functional structures or surface-energy-controlled surfaces [10,20]. Indeed, many super-hydrophilic or super-hydrophobic surfaces are based on high-aspect-ratio (~15) structures whose surfaces can be effectively engineered by ALD [10,21]. The surface properties of ALD TiO_2 may also be altered by various treatment techniques which, however, have been rarely reported as of yet.

In this paper, we demonstrate control of the surface properties of ALD TiO_2 thin films by using an ultraviolet (UV) light treatment. Contact angle analysis shows that the wettability of ALD TiO_2 surfaces is strongly dependent on the UV treatment time. More importantly, the wettability is largely dominated by ALD process parameters such as the deposition temperature as well as the thickness of the films; only relatively thick ALD TiO_2 samples deposited at high temperature (200 °C) showed super-hydrophilicity (water contact angle < 1°) after an extended UV treatment. Micromorphological and compositional analysis show that such dependence may be closely relevant to the bandgap energy and the defect concentration in the film, affecting the electron–hole pair generation and the carrier recombination, respectively.

* Corresponding author at: Department of Manufacturing Systems and Design Engineering, Seoul National University of Science and Technology, 232 Gongneung-ro, Nowon-gu, Seoul 01811, South Korea.
E-mail address: jihwanan@seoultech.ac.kr (J. An).

http://dx.doi.org/10.1016/j.tsf.2017.09.028
Received 20 April 2017; Received in revised form 8 September 2017; Accepted 13 September 2017
Available online 15 September 2017

2. Experimental section

TiO_2 films were grown on p-type Si (100) wafers in a travelling-wave-type customized ALD station. Titanium (IV) isopropoxide (TTIP (97%), Alfa Aesar $C_{12}H_{28}O_4Ti$) was used for the Ti precursor, H_2O was used for the oxidant, and N_2 was used for the purging gas at 20 sccm. TTIP and H_2O were kept at 50 °C and at room temperature, respectively. The base pressure was 67 Pa. The pulsing times were 1 s for the TTIP and 0.1 s for the H_2O. To investigate the effect of the deposition temperature on ALD TiO_2 thin films, the deposition temperatures were set to 75 °C, 125 °C, and 200 °C at a thickness of 16 nm. To investigate the effect of film thickness, the thicknesses of the films were varied as 6 nm, 11 nm, and 16 nm at the deposition temperature of 200 °C.

To measure the in situ wettability change of the ALD TiO_2 thin-film surface under UV irradiation, contact angle measurements were performed using an optical contact angle meter (CAM-200, KSV Instruments) with 10-μL drops of de-ionized water from 0 min to 15 min at the interval of 1 min. A black-light UV lamp (F4 T5/BLB 4-W, Sankyo, 365-nm wavelength) was used as a luminous source with an intensity of ~3 mW/cm^2. This value is comparable to the UV intensity range of sunlight (~1 mW/cm^2) [22].

Optical properties including the refractive index (n) and extinction coefficient (k) were obtained from the analysis by using a spectroscopic ellipsometer (M2000D, Woollam). The ellipsometry spectra were measured within the wavelength range of 200–1600 nm. The extinction coefficient determines the adsorption coefficient (α). The optical bandgap was obtained from a Tauc plot based on the adsorption coefficient data.

The surface morphology of the ALD TiO_2 films was characterized by atomic force microscopy (AFM, SmartSPM-1000 AIST-NT). The crystallinity and phase of the ALD TiO_2 films were determined by grazing incidence X-ray diffraction (GIXRD) measurements (Bruker DE/D8 Advance, Bruker) at an angle range from 20° to 80°, incident angle of 1°, step size of 0.04°, and scan speed of 2 s/step. The composition of the films was characterized by X-ray photoelectron spectroscopy (XPS) with an Al Kα source, a spot size of 400 μm^2, a step size of 1 eV/step, and a binding energy range of 0–1200 eV. Bright-field cross-sectional transmission electron microscopy (TEM) characterization was performed with the sample prepared by a Cs-corrected transmission electron microscope (JEM-ARM200F, JEOL) at the acceleration voltage of 200 kV. The thickness and optical properties of the ALD TiO_2 thin films were evaluated by a spectroscopic reflectometer (ST5000-Auto200).

3. Results and discussion

Fig. 1 shows the water contact angle measurement results on the 16-nm-thick ALD TiO_2 film on a Si substrate deposited at 75 °C, 125 °C, and 200 °C upon UV irradiation. The water contact angle measurements were conducted after several weeks in dark and vacuum environments after deposition so that the TiO_2 surface became hydrophobic [23]. Indeed, the water contact angles of the ALD TiO_2 film surfaces before UV irradiation were > 80° (hydrophobic surfaces), regardless of the deposition temperature. Surface contamination was not significant as < 2% of carbon on the surface from X-ray photoelectron spectroscopy (XPS) analysis. As was pointed out by Huang et al., the initial hydrophobicity after storage in vacuum is due to the loss of the absorbed molecules and the restoration from initially OH-terminated surfaces, which was much faster in vacuum than in air due to the lack of H_2O [9]. In the reference samples (75 °C and 200 °C samples without UV exposure), the contact angle consistently decreased at the rate of 3.0–3.2°/min. Considering that photocatalytic activity rarely occurs without UV light, the decrease in contact angle seems to be due to an evaporation-induced volume change. Park et al. reported that the contact line is pinned and the contact angle linearly drops when the ratio between the collapsed time and the time for complete evaporation is small (stage 1) for single isolated evaporating droplets, as in our measurements [24]. The fact that no recession of the droplet borderline is observed also implies that our measurements were taken at stage 1. Upon UV irradiation, the water contact angle in the sample deposited at < 200 °C linearly decreased at the rate of 3.8°/min and 3.3°/min for the 75 °C and 125 °C samples, respectively, which are not different from the reference samples; the decrease in contact angle in these samples is also mainly due to evaporation. Interestingly, however, the water contact angle of ALD TiO_2 deposited at the relatively high temperature of 200 °C dramatically decreased upon UV irradiation (24.6°/min for the first 3 min); the surface became super-hydrophilic (water contact angle of 11.8° only after 3 min, and < 1° after 8 min). These results clearly show that the deposition temperature significantly affects the wettability of the ALD TiO_2 film surface upon UV treatment.

Fig. 2 shows the water contact angle measurement results of ALD TiO_2 films of 6-nm, 11-nm, and 16-nm thicknesses deposited at 200 °C upon UV irradiation. In this set of samples, the contact angles on the reference samples (6-nm and 16-nm samples without UV exposure) gently and linearly dropped at the rate of 3.1–3.2°/min. The 16-nm sample shows a dramatic decrease in the contact angle as was discussed in the previous paragraph (24.6°/min for the first 3 min). The 6-nm and 11-nm samples, however, do not show such an abrupt change to a super-hydrophilic surface. Their contact angles rather gently decreased at the rate of 3.9°/min and 4.7°/min for the 6-nm and 11-nm samples, respectively, which are faster than the reference samples.

Because the roughness of the sample surface may significantly affect the wetting property observed in Figs. 1 and 2, we have analyzed the surface morphologies of the ALD TiO_2 films. AFM analysis results (Fig. 3(a)–(e)) show that the surface of the samples are all extremely

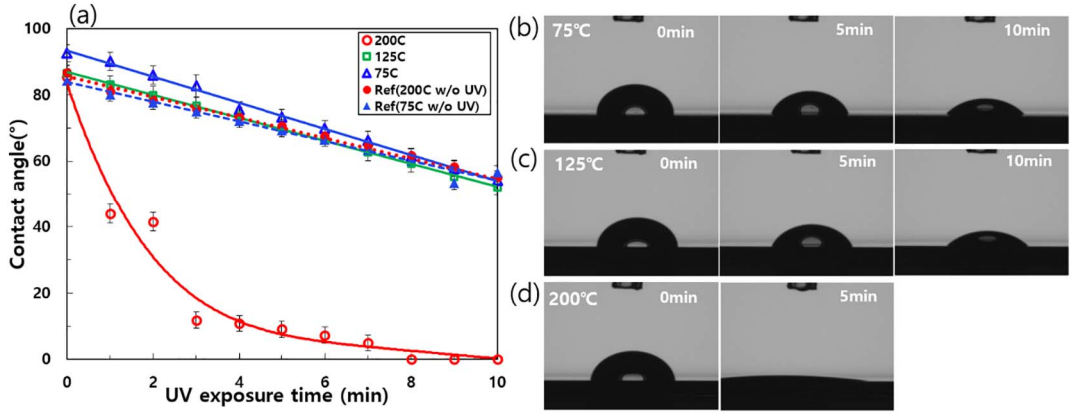

Fig. 1. Contact angle vs. UV exposure time curves of ALD TiO_2 films (16 nm thick) deposited at various temperatures: (a) summary and captured images of (b) 75 °C, (c) 125 °C, and (d) 200 °C samples at varying UV exposure times.

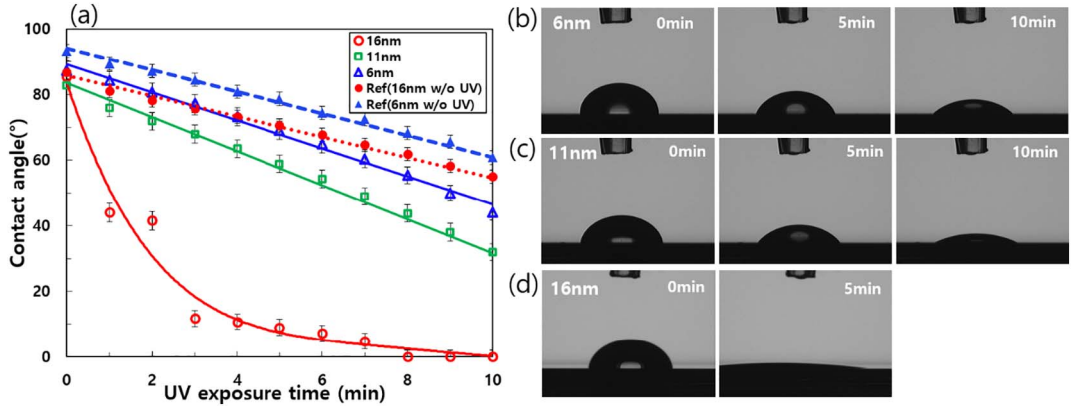

Fig. 2. Contact angle vs. UV exposure time curves of ALD TiO_2 films (deposition temperature of 200 °C) deposited at various thicknesses: (a) summary and captured images of (b) 6-nm-, (c) 11-nm-, and (d) 16-nm-thick samples at varying UV exposure times.

smooth with the RMS roughness of < 0.3 nm regardless of the deposition temperature and film thicknesses(Fig. 3(f)). We further conducted XRD analysis to confirm the relation between the deposition temperature, the thickness, and the crystallinity. Fig. 3(g) shows the GIXRD results of the samples. ALD TiO_2 films deposited at temperatures < 200 °C show an amorphous phase, as was also shown in other literature [11,25,27]. Only the relatively thick (16 nm) sample deposited at high temperature (200 °C) shows strong crystalline anatase peaks: peaks are observed at 25.1° and 47.9°, which correspond to (101) and (200) planes of anatase TiO_2, respectively [25,28,29]. 6-nm and 11-nm samples deposited at 200 °C also show the (200) peak at 47.9°, which, however, even weaker than that of the 16-nm sample. Aarik et al. previously reported the similar trend regarding the crystallinity of ALD TiO_2 films depending on the deposition temperature and the film thickness: only those grown at T ≥ 165 °C and having sufficient thickness (≥ 15 nm) showed diffraction patterns characteristic to polycrystalline TiO_2 [26]. Kessels et al. also reported a transition phenomenon from an amorphous phase to a crystalline (anatase) phase in ALD TiO_2 films of ~10 nm in thickness deposited at 300 °C. They determined that the transition is dependent not only on the deposition temperature, but also on the thickness [27].

Fig. 4 shows the cross-sectional TEM images of ALD TiO_2 films deposited on Si wafers. TiO_2 films are deposited on the native oxide layers (white layer in the TEM image) of 2–3 nm in thickness. TEM results correspond well to the XRD results shown in Fig. 3: a primarily anatase phase is shown in the 16-nm sample deposited at 200 °C, while all other samples are mostly amorphous. The *d*-spacing in the 200 °C, 16-nm sample was measured to be 0.337 nm, which agrees with the *d*-spacing of (101) planes (0.339 nm) of anatase-phase TiO_2 ($a = b = 0.378–0.379$ nm, $c = 0.950–0.952$ nm) [6,17,18,22,29].

Fig. 5 shows the bandgap energy (E_g) and refractive index depending on the deposition temperature and the film thickness. The optical absorption strength is related to the photon energy and bandgap with the following relation:

$$(\alpha h\nu)^{1/n} = A(h\nu - E_g)$$

where α is the absorption coefficient ($\alpha = 4\pi\kappa/\lambda$), h is Planck's constant, E_g is the bandgap energy, A is a proportionality coefficient, and n in the exponent is determined by the electronic transition property: when the TiO_2 is anatase phase or amorphous as in our samples, the nature of the electronic structure allows for indirect transitions, which implies $n = 2$ [31,32,43]. One can calculate the bandgap energy (E_g) using a Tauc plot, and the results are shown in Fig. 5(a) and (b) [12–16,27,29–37]. The bandgap energies of the 16-nm-thick samples deposited at 75 °C, 125 °C, and 200 °C are 3.48 eV, 3.31 eV, and 3.22 eV, respectively (Fig. 5(a)). The bandgap energy tends to decrease as the deposition temperature increases. Huang et al. also reported a similar trend at deposition temperatures below 300 °C [23]. The bandgap energy also decreased as the film thickness was increased which, however, is even less compared to the deposition temperature dependence and well below the photon energy (3.4 eV) of the UV light (3.25 eV, 3.24 eV, and 3.18 eV for 6-nm, 11-nm, and 16-nm samples, respectively). Heikkilä et al. previously reported that the bandgap energy changes little, if at all, as a function of the thickness [30]. The refractive index was also dominated by both the deposition temperature and the film thickness. The refractive index decreases depending on the temperature: 2.05, 2.32, and 2.47 for 75 °C, 125 °C, and 200 °C samples, respectively, which corresponds well with a previous report [23]. The thickness also determines the refractive index: 2.26, 2.38, and 2.55 for 6-nm, 11-nm, and 16-nm samples, respectively. The refractive index of TiO_2 is known to be largely affected by the density [39,40]; i.e., a low refractive index seems to imply a low film density, possibly due to the large

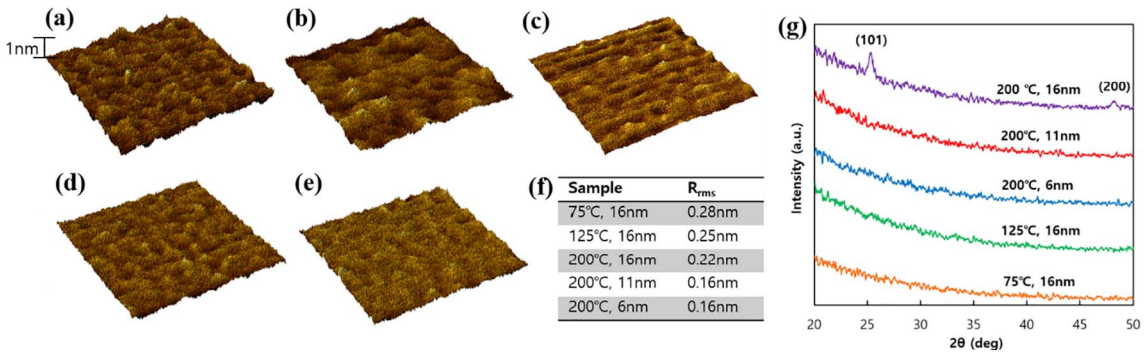

Sample	R_{rms}
75°C, 16nm	0.28nm
125°C, 16nm	0.25nm
200°C, 16nm	0.22nm
200°C, 11nm	0.16nm
200°C, 6nm	0.16nm

Fig. 3. AFM and XRD analysis results of the ALD TiO_2 films on Si wafer: AFM images of (a) 75 °C/16 nm, (b) 125 °C/16 nm, (c) 200 °C/16 nm, (d) 200 °C/11 nm, and (e) 200 °C/6 nm samples, and (f) the summary of RMS roughness of the samples. *Z*-scales and analyzing area sizes are identical for all images (analyzing area: 200 nm × 200 nm). (g) XRD spectra of the samples.

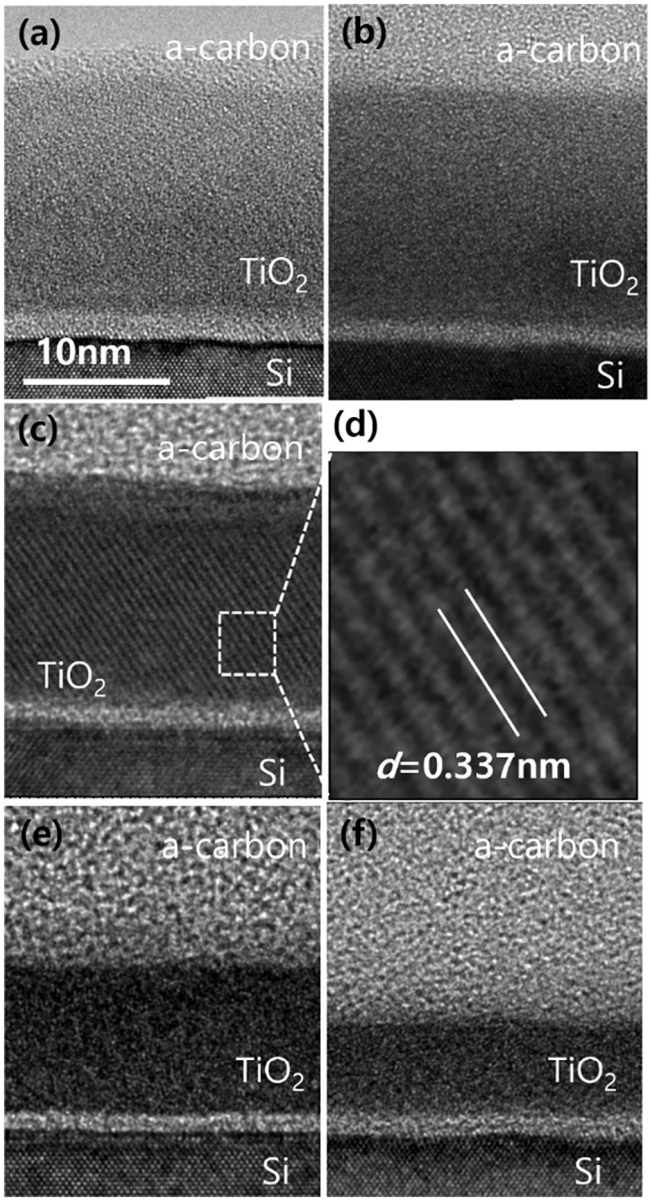

Fig. 4. TEM images of ALD TiO_2 samples on Si substrates: (a) 75 °C, 16 nm, (b) 125 °C, 16 nm, (c) 200 °C, 16 nm, (d) zoom-in image of 200 °C, 16-nm sample, (e) 200 °C, 11 nm, and (f) 200 °C, 6 nm. White region between TiO_2 film and Si substrate is the native SiO_2 (~2 nm thick).

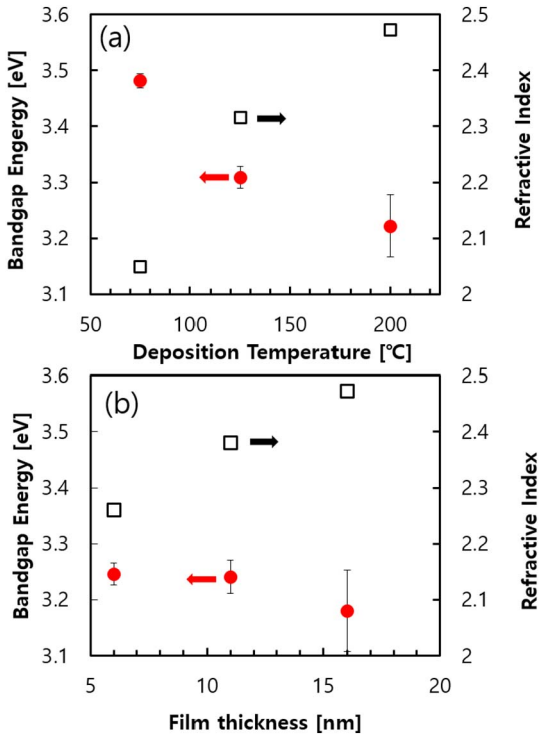

Fig. 5. Bandgap energy and refractive index (at 550 nm) of ALD TiO_2 films: (a) depending on the deposition temperature (at a thickness of 15 nm) and (b) depending on the film thickness (at a deposition temperature of 200 °C).

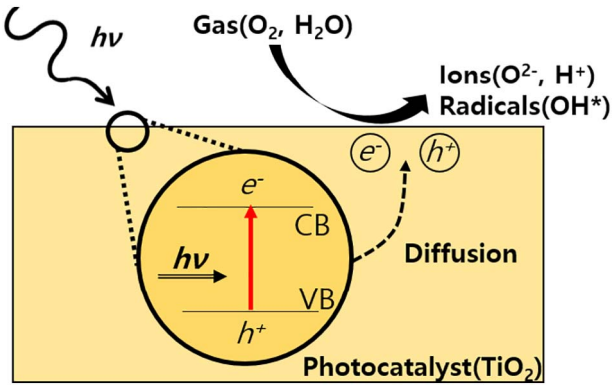

Fig. 6. Schematic showing the individual steps in the photocatalytic reaction near the ALD TiO_2 film surface.

concentration of bulk defects. Bulk defects function as recombination sites for charge carriers such as holes and electrons, and therefore, can impede the facile diffusion of the carriers from the generation site to the film surface [41–43].

The hydrophilicity of the ALD TiO_2 surface upon UV exposure in Figs. 1 and 2 can be understood based on the photocatalytic activity associated with the crystallinity (Figs. 3 and 4) and the optical measurement (Fig. 5) results. The photocatalytic activity upon UV exposure can be described by the following mechanism (Fig. 6) [8]: 1) the electron–hole pair is generated upon the incidence of light whose energy is higher than the bandgap of the photocatalyst ($TiO_2 + h\nu \rightarrow e^- + h^+$), 2) electrons and holes diffuse to the surface, and 3) electrons and holes at the surface react with O_2, H_2O, etc., generating ions (O^{2-}, H^+) or radicals (OH*) ($e^- + O_2 \rightarrow O^{2-}$, $h^+ + H_2O \rightarrow OH^* + H^+$). High-energy radicals generated at the surface increase the surface energy so that the water contact angle decreases; i.e., the surface becomes more hydrophilic.

The changes in bandgap energy and refractive index (or defect density) shown in Fig. 5 may have affected the evolution of the hydrophilicity (Figs. 1 and 2) based on the mechanism above. First, the lower bandgap energy and the decreased bulk defects in the sample deposited at higher temperatures (Fig. 5(a)) may have generated more electron–hole pairs and lessened the carrier recombination during diffusion, respectively. As a result, more carriers have diffused to the surface, generated more ions or radicals, and increased the surface energy. As a result of the two effects combined, the wettability change in the 200 °C sample was significantly different from that in the 75 °C and the 125 °C samples. Second, the thicker sample showed a slightly lower bandgap energy as well as a much larger refractive index, which can also cause more electron–hole pair generation and less recombination. In this case, however, the change in the refractive index owing to the bulk defect density was more dominant compared to that of the bandgap energy; the bandgap energies were similar between the samples with different thicknesses, all of which are lower than the photon energy (3.4 eV). This implies that the hydrophilicity evolution

in the samples with different thicknesses may be largely due to the different recombination probability [33,37,38,40–42]. It should be also noted that the existence of O_2 or H_2O in the atmosphere is essential in the evolution of the hydrophilicity; indeed, the hydrophilicity was not observed in the similar experiment conducted in vacuum, i.e., in the absence of O_2 or H_2O [23].

The wettability control, and therefore, surface energy control, of the ALD TiO_2 film surface in this paper has implications for the deposition of films or particles on the surface. For instance, there are 3 different growth modes when one deposits films on a substrate with a vapor deposition method depending on the interfacial free energy at the substrate–vapor (γ_{SV}), film–substrate (γ_{FS}), and film–vapor (γ_{FV}) interfaces: the film grows either layer-by-layer (Frank–van der Merwe (FM) mode, $\gamma_{SV} > \gamma_{FS} + \gamma_{FV}$), in island clusters (Volmer–Weber (VW) mode, $\gamma_{SV} \leqq \gamma_{FS} + \gamma_{FV}$), or in mixed-layer clusters (Stranski–Krastanov (SK) mode), depending on the surface energy relationship [44]. Therefore, one can tune the parameters such as thickness, size, distribution, etc. of films or particles by controlling the wettability or surface energy using a UV treatment on the ALD TiO_2 surface which, for example, could be beneficial for realizing high-surface-area nanoscale structures. Further studies in this aspect are still on-going.

4. Conclusion

We showed the wettability control of an ALD TiO_2 surface using an UV treatment. We confirmed that the deposition temperature and film thickness are the factors governing the crystallinity of the films, altering the bandgap energy and the bulk defect density and, therefore, affecting the electron–hole pair generation and the carrier recombination. The UV-induced wettability control of ALD TiO_2 surface reported in this paper may have great implications in various engineering applications that employ interfaces associated with ALD TiO_2.

Acknowledgement

We acknowledge the financial support from the National Research Foundation under the Ministry of Education, Korea (NRF-2015R1D1A1A01058963). We also acknowledge the financial support by the Ministry of Trade, Industry and Energy (MOTIE), KOREA, through the Education Support program for Creative and Industrial Convergence. (Grant Number N0000717). We thank Si Hwan Kim, Kwonil Seong and Prof. Hyo-Sok Ahn for the assistance in AFM measurements.

References

[1] H.A. Macleod, Thin-Film Optical Filters, fourth ed., CRC Press, New York, 2009.
[2] A. Szeghalmi, M. Helgert, R. Brunner, F. Heyroth, U. Gosele, M. Knez, Atomic layer deposition of Al_2O_3 and TiO_2 multilayers for applications as bandpass filters and antireflection coatings, Appl. Opt. 48 (2009) 1727–1732.
[3] Y. Kim, P. Schindler, A.L. Dadlani, S. Acharya, J. Provine, J. An, F.B. Prinz, Plasma-enhanced atomic layer deposition of barium titanate with aluminum incorporation, Acta Mater. 117 (2016) 153–159.
[4] S.K. Kim, W.D. Kim, K.M. Kim, C.S. Hwang, High dielectric constant TiO_2 thin films on a Ru electrode grown at 250 °C by atomic layer deposition, Appl. Phys. Lett. 85 (2004) 4112–4114.
[5] J. An, T. Usui, M. Logar, J. Park, D. Thian, S. Kim, K. Kim, F.B. Prinz, Plasma processing for crystallization and densification of atomic layer deposition $BaTiO_3$ thin films, ACS Appl. Mater. Interfaces 6 (2014) 10656–10660.
[6] C. Clement Raj, R. Prasanth, A critical review of recent developments in nanomaterials for photoelectrodes in dye sensitized solar cells, J. Power Sources 317 (2016) 120–132.
[7] R. Wang, K. Hashimoto, A. Fusjishima, M. Chikuni, E. Jojima, A. Kitamura, M. Shimohigoshi, T. Watanabe, Light-induced amphiphilic surfaces, Nature 388 (1997) 431–432.
[8] R. Thiruvenkatachari, S. Vigneswaran, I.S. Moon, A review on UV/TiO2 photocatalytic oxidation process, Korean J. Chem. Eng. 25 (2008) 64–72.
[9] T. Zubkov, D. Stahl, T.L. Thompson, D. Panayotov, O. Diwald, J.T. Yates Jr., Ultraviolet light-induced hydrophilicity effect on TiO_2. Dominant role of the photooxidation of adsorbed hydrocarbons causing wetting by water droplets, J. Phys. Chem. B 109 (2005) 15454–15462.
[10] P. Banerjee, I. Perez, L. Henn-Lecordier, S.B. Lee, G.W. Rubloff, Nanotubular metal–insulator–metal capacitor arrays for energy storage, Nat. Nanotechnol. 37 (2009) 292–296.
[11] K.E. Tettey, M.I. Dafinon, D. Lee, Progress in superhydrophilic surface development, Mater. Express 1 (2011) 89–104.
[12] P. Chinnamuthu, A. Mondal, N.K. Singh, J.C. Dhar, K.K. Chattopadhyay, S. Bhattacharya, Band gap enhancement of glancing angle deposited TiO_2 nanowire array, J. Appl. Phys. 112 (2012) 054315.
[13] C. Yu, L. Wei, J. Chen, Y. Xie, W. Zhou, Q. Fan, Enhancing the photocatalytic performance of commercial TiO_2 crystals by coupling with trace narrow-band-gap Ag_2CO_3, Ind. Eng. Chem. Res. 53 (2014) 5759–5766.
[14] K. Gupta, R.P. Singh, A. Pandey, A. Pandey, Photocatalytic antibacterial performance of TiO_2 and Ag-doped TiO_2 against *S. aureus*. *P. aeruginosa* and *E. coli*, Beilstein J. Nanotechnol. 4 (2013) 345–351.
[15] H.P. Quiroz, A. Dussan, Synthesis of self-organized TiO_2 nanotube arrays: microstructural, stereoscopic, and topographic studies, J. Appl. Phys. 120 (2016) 051703.
[16] S. Kurian, H. Seo, H. Jeon, Significant enhancement in visible light absorption of TiO2 nanotube arrays by surface band gap tuning, J. Phys. Chem. C 117 (2013) 16811–16819.
[17] M. Amjadi, S. Rowshanzamir, S.J. Peighambardoust, M.G. Hosseini, M.H. Eikani, Investigation of physical properties and cell performance of nafion/TiO_2 nanocomposite membranes for high temperature PEM fuel cells, Int. J. Hydrog. Energy 35 (2010) 9252–9260.
[18] Z. Wang, H. Tang, M. Pan, Self-assembly of durable nafion/TiO_2 nanowire electrolyte membranes for elevated-temperature PEM fuel cells, J. Membr. Sci. 369 (2011) 250–257.
[19] W. Dong, K. Zhang, Y. Zhang, T. Wei, Y. Sun, X. Chen, N. Dai, Application of three-dimensionally area-selective atomic layer deposition for selectively coating the vertical surfaces of standing nanopillars, Sci Rep 4 (2014) 4458.
[20] P. Schindler, M. Logar, J. Provine, F.B. Prinz, Enhanced step coverage of TiO_2 deposited on high aspect ratio surfaces by plasma-enhanced atomic layer deposition, Langmuir 31 (2015) 5057–5062.
[21] G. Vereecke, X.M. Xu, W.K. Tsai, H. Yang, S. Armini, T. Delande, G. Doumen, F. Kentie, X. Shi, I. Simms, K. Nafus, F. Holsteyns, H. Struyf, S. De Gendt, Partial wetting of aqueous solutions on high aspect ratio nanopillars with hydrophilic surface finish, ECS J. Solid State Sci. Technol. 3 (2014) 3095–3100.
[22] K.N. Liou, An Introduction to Atmospheric Radiation, Academic press, California, 2002.
[23] Y. Huang, G. Pandraud, P.M. Sarro, Characterization of low temperature deposited atomic layer deposition TiO_2 for MEMS applications, J. Vac. Sci. Technol. A 31 (2013) 01A148.
[24] J.K. Park, J. Ryu, B.C. Koo, S. Lee, K.H. Kang, How the change of contact angle occurs for an evaporating droplet: effect of impurity and attached water films, Soft Mater. 8 (2012) 11889–11896.
[25] H.E. Cheng, C.C. Chen, Morphological and photoelectrochemical properties of ALD TiO_2 films, J. Electrochem. Soc. 155 (2008) 604–607.
[26] J. Aarik, A. Aidla, T. Uustare, V. Sammelselg, Morphology and structure of TiO_2 thin films grown by atomic layer deposition, J. Cryst. Growth 148 (1995) 268–275.
[27] E. Langereis, S.B.S. Heil, H.C.M. Knoops, W. Keuning, M.C.M. Van de Sanden, W.M.M. Kessels, In situ spectroscopic ellipsometry as a versatile tool for studying atomic layer deposition, J. Phys. D. Appl. Phys. 42 (2009) 073001.
[28] S.K. Kim, S. Hoffmann-Eifert, M. Reiners, R. Waser, Relation between enhancement in growth and thickness-dependent crystallization in ALD TiO_2 thin films, J. Electrochem. Soc. 158 (2011) 6–9.
[29] L. Miao, P. Jin, K. Kaneko, A. Terai, N. Nabatova-Gabain, S. Tanemura, Preparation and characterization of polycrystalline anatase and rutile TiO_2 thin films by RF magnetron sputtering, Appl. Surf. Sci. 212-213 (2003) 255–263.
[30] M. Heikkilä, E. Puukilainen, M. Ritala, M. Leskelä, Effect of thickness of ALD grown TiO_2 films on photoelectrocatalysis, J. Photochem. Photobiol. A Chem. 204 (2009) 200–208.
[31] B.D. Viezbicke, S. Patel, B.E. Davis, D.P. Birnie III, Evaluation of the Tauc method for optical absorption edge determination: ZnO thin films as a model system, Phys. Status Solidi B 252 (2015) 1700–1710.
[32] D.M. King, X. Du, A.S. Cavanagh, A.W. Weimer, Quantum confinement in amorphous TiO_2 films studied via atomic layer deposition, Nanotechnology 19 (2008) 445401.
[33] M. Zhang, G. Lin, C. Dong, L. Wen, Amorphous TiO_2 films with high refractive index deposited by pulsed bias arc ion plating, Surf. Coat. Technol. 201 (2007) 7252–7258.
[34] D. Mardare, P. Hones, Optical dispersion analysis of TiO_2 thin films based on variable-angle spectroscopic ellipsometry measurements, Mater. Sci. Eng. B 68 (1999) 42–47.
[35] S. Tanemura, L. Miao, W. Wunderlich, M. Tanemura, Y. Mori, S. Toh, K. Kaneko, Fabrication and characterization of anatase/rutile–TiO_2 thin films by magnetron sputtering: a review, Sci. Technol. Adv. Mater. 6 (2005) 11–17.
[36] S.J. Park, J.P. Lee, J.S. Jang, H. Rhu, H. Yu, B.Y. You, C.S. Kim, K.J. Kim, Y.J. Cho, S. Baik, W. Lee, In situ control of oxygen vacancies in TiO_2 by atomic layer deposition for resistive switching devices, Nanotechnology 24 (2013) 295202.
[37] N.R. Mathews, E.R. Morales, M.A. Corte's-Jacome, J.A. Toledo Antonio, TiO_2 thin films – influence of annealing temperature on structural, optical and photocatalytic properties, Sol. Energy 83 (2009) 1499–1508.
[38] A. Taherniya, D. Raoufi, The annealing temperature dependence of anatase TiO_2 thin films prepared by the electron-beam evaporation method, Semicond. Sci. Technol. 31 (2016) 125012.
[39] D. Mergel, D. Buschendorf, S. Eggert, R. Grammes, B. Samset, Density and refractive index of TiO_2 films prepared by reactive evaporation, Thin Solid Films 371 (2000)

218–224.
[40] Y.M. Chiang, D. Birnie, D.W. Kingery, Physical Ceramics: Principles for Ceramics Science and Engineering Principles for Ceramic Science, second ed., Wiley, New Jersey, 1996.
[41] Q. Xiang, J. Yu, P.K. Wong, Quantitative characterization of hydroxyl radicals produced by various photocatalysts, J. Colloid Interface Sci. 357 (2011) 163–167.
[42] B. Liu, K. Nakata, X. Zhao, T. Ochiai, T. Murakami, A. Fujishima, Theoretical kinetic analysis of heterogeneous photocatalysis: the effects of surface trapping and bulk recombination through defects, J. Phys. Chem. C 115 (2011) 16037–16042.
[43] T. Luttrell, S. Halpegamage, J. Tao, A. Kramer, E. Sutter, M. Batzill, Why is anatase a better photocatalyst than rutile? - model studies on epitaxial TiO_2 films, Sci Rep 4 (2014) 4043.
[44] G.H. Gilmer, H. Huang, C. Roland, Thin film deposition: fundamentals and modeling, Comput. Mater. Sci. 12 (1998) 354–380.